Transition Effect on the Shock Wave / Boundary Layer Interaction Region and the Wake at Low Supersonic Mach Number

*Pavel A. Polivanov**, Andrey A. Sidorenko** and Anatoly A. Maslov**
**Khristianovich Institute of Theoretical and Applied Mechanics SB RAS*
630090, Institutskaya, 4/1, Novosibirsk, Russia
***Novosibirsk State University*
630090, Pirogova, 2, Novosibirsk, Russia

Abstract
The paper deals with an experimental study of effect of laminar, transitional and turbulent boundary layer on stationary and non-stationary characteristics of the shock wave / boundary layer interactions (SWBLI) and wake. Incident shock wave generated by a wedge induced the separation of the boundary layer developed on the flat plate. The boundary layer state was varied from laminar to turbulent by changing position of the interaction relative to the leading edge. The measurements were performed by PIV. It was found that the growth of the momentum thickness and coherent structures in wake strongly depends on the state of the incoming boundary layer.

1. Introduction

Modern trends in transonic aviation are connected with reducing of viscous drag. Therefore commercial airplanes of the next generations may be equipped with a laminar wing [1,2]. Generic feature of the transonic flow near the airfoil is presence of local supersonic zone ended by a shock wave. Laminar boundary layer has weak resistance to adverse pressure gradients especially ones produced by shock waves, in contrast to the turbulent boundary layer [3]. This leads to significant flow separation that can eliminate all advantages of laminar flow. Therefore it is necessary to estimate the difference between steady and unsteady parameters of the separation zone for various positions of the laminar-turbulent transition relative to the zone of shock wave boundary layer interaction (SWBLI) for moderate Mach numbers. Flow separation on airfoil not only reduce the lifting force and increases drag, but also leads to additional adverse events, including buffeting [3]. It is well known that separation of laminar flow has a greater length as compared to turbulent [4, 5]. The goal of this investigation is an experimental study of the SWBLI at different regimes of inflow boundary layer from laminar to turbulent.

2. Wind tunnel experiments

2.1 Experimental setup

The experiments were performed in wind tunnel T-325 (ITAM SB RAS) for Mach number M_∞ = 1.47, total temperature 291 K and four values of total pressure P_0 = 0.55, 0.7, 0.85 and $1.0 \cdot 10^5$ Pa ($Re_1 = 8.5\text{-}15.5 \cdot 10^6$ m^{-1}). Test chamber of the wind tunnel has a rectangular cross section of 160x200 mm. The configuration of the experimental model is presented in Figure 1 (a). Experimental model consisted of a plate with sharp leading edge occupying full span of the test section and a wedge generating a shock wave. In this series of experiments, the wedge angle was 4º. This corresponds to regular reflection of a shock wave from a model for the inviscid case. The blockage ratio of the test section was relatively high therefore the flow start was provided by extended cavities above the wedge and below the plate. Variation of local boundary layer parameters and its state (laminar/turbulent) was provided by shifting of the flat plate in streamwise direction relatively to the wedge. To provide the same conditions near the leading edge the extension plates were installed downstream of the lower nozzle wall. Several extension plates of different length L were used. The figure shows that the distance from the flat plate leading edge to the center of the optical window is connected with length of the extension plate and is approximately equal to (380-L) mm. Position of the wedge was chosen to provide intersection of the shock wave with the model approximately in the center of the optical window. The effect of natural laminar-turbulent transition on stationary and non-stationary parameters of the SWBLI was studied for three cases L = 100, 200 and 250 mm (Approximate distance from the leading edge to the

intersection the incident shock wave with the model was equal to 285, 185 and 135 mm respectively). Study of the effect of the surface roughness shape and its location was carried out for the case of L = 250 mm and the stagnation pressure $P_0 = 0.7 \cdot 10^5$ Pa. In the current study two types of roughness were considered (Fig. 1b). The first type was a straight strip with rectangular cross-section (# 1, # 2, # 4) and the second was a zig-zag strip (# 3, # 5, # 6). As can be seen from the figure several parameters of the roughness were varied namely thickness, width, plane shape and location relative to the leading edge.

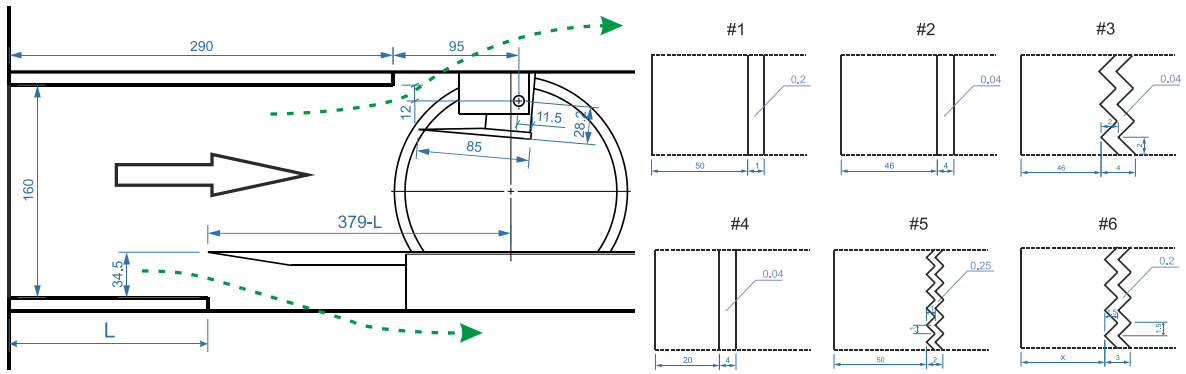

Figure 1 : The draft of a) experimental model and b) roughness

The main measurement techniques were PIV, Schlieren visualization and measurements of wall pressure by steady pressure sensors arranged along the model. DEHS microparticles with an average size of 1 micron were used for PIV measurement. The velocity field was reconstructed from tracer images by means of the cross-correlation adaptive algorithms with continuous sliding of interrogation window and grid refinement of the interrogation cells. Mean velocity distributions and distributions of unsteady characteristics were obtained on the basis of 4000-5000 instant velocity fields.

Hot-wire probe and Pitot tube (outer diameter of 0.3 mm) were used to determine the position of the laminar-turbulent transition. The sensors were traversed streamwise at a fixed distance from the wall (for the hot-wire the distance was 0.25 mm, and the Pitot tube touched the surface). It was found that the beginning of the transition changes from 150 to 120 mm with increasing of Reynolds number and the end of the transition changes from 210 to 180 mm. Along the transverse coordinate position of transition slightly varied in the range of 15-20 mm. These data indicate that using of extension plate of length L = 250 mm provided laminar inflow boundary layer for all Reynolds numbers. For the case of L = 200 mm the inflow boundary layer was transitional and for L = 100 mm the boundary layer was turbulent.

2.2 Experimental results

Figure 2 presents the examples of the mean flow in SWBLI region for different states of the inflow boundary layer. For the case of fully turbulent interaction it is possible to see the formation of strong Mach stem (Figure 2a). Mach stem is generated here due to presence of strong reflected (separated) shock wave. This leads to considerable increase of the local adverse pressure gradient. It is interesting to note that the cause of the formation of a strong shock wave is higher resistance of the turbulent boundary layer to the separation. Due to this the length of separation bubble is relatively small and therefore in the zone of SWBLI there is very rapid growth of the displacement thickness of boundary layer. This leads to the formation of a strong reflected shock wave.

If the inflow boundary layer is laminar (Figure 2c) significant increase of the interaction zone length was obtained. In this study the classic laminar flow separation was not obtained, because of adverse pressure gradient caused earlier laminar-turbulent transition. From the RMS velocity distribution it can be assumed that the transition occurs near the point of intersection of the incident shock wave with the model. The main increase of wall pressure occurs in this region that leads to growth of flow pulsations. Laminar-turbulent transition in the interaction region leads to significant reduction of its length compared to the classical laminar case. It is accompanied by higher level of fluctuations in the interaction zone and the downstream region.

The figure shows that for the laminar case the growth of the displacement thickness of the boundary layer is less intensive in comparison with the turbulent case. This leads to formation of weak compression waves instead of a strong shock wave in the turbulent case. As a result the strong Mach stem was not found in the laminar test case.

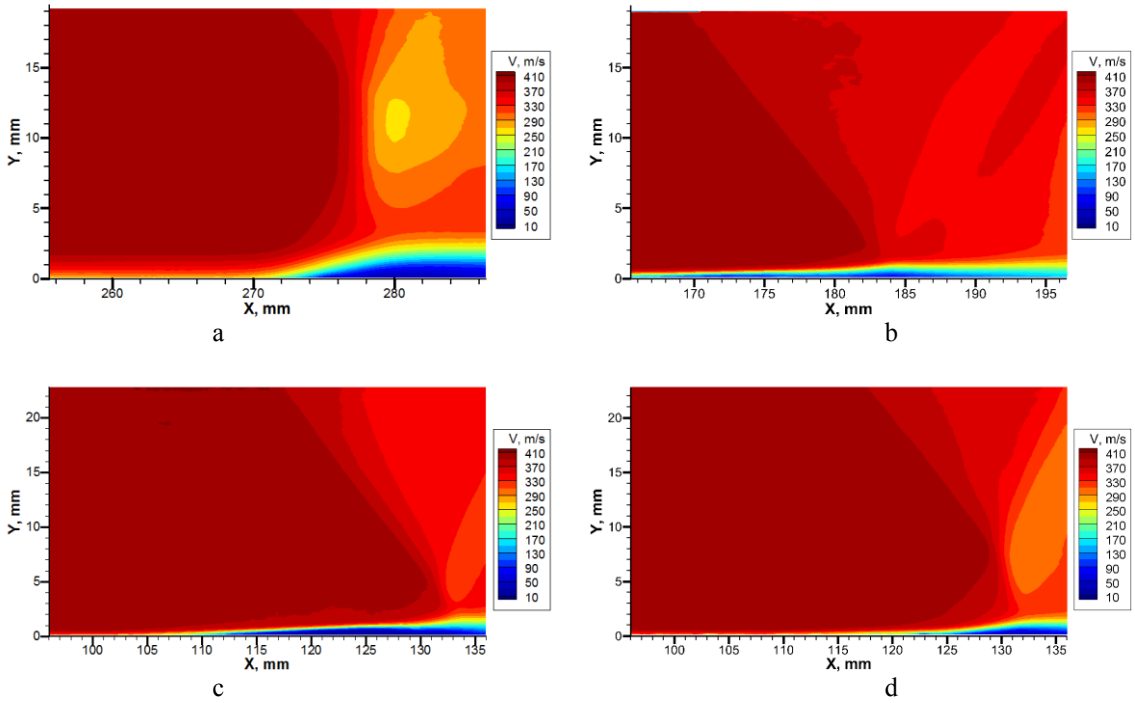

Figure 2 Mean velocity fields for different inflow boundary layer: a) turbulent, b) transitional, c) laminar d) laminar with roughness

Figure 2b shows the velocity field obtained near the end of the laminar-turbulent transition zone. It is clearly seen that in this case there is no formation of strong reflected shock wave despite the small length of SWBLI region. Therefore the transitional inflow boundary layer corresponds to the most favorable interaction conditions. Small length of the interaction region is connected with a sharp increase of the fullness of the velocity profile. Absence of strong reflected (separation) shock wave is possible due to slow receptivity of SWBLI zone to the state of the inflow boundary layer [6, 7].

Parameters of experiments carried out in natural laminar-turbulent transition are shown in Table 1. From the table it can be seen that the Mach number upstream of SWBLI (calculated on the basis of PIV data) is less than the measured upstream of the model (M = 1.47). This can be explained by a decrease of the Mach number in a weak wave generated by the leading edge of the plate, which crosses the flow several times due to its reflections from the walls. The value of X_{imp} corresponds to the point of intersection of the incident shock wave with plate for the inviscid flow, measured from the leading edge of the plate.

Table 1 Parameters of experiments

M	P_0, bar	T_0, K	Re_1, 10^6	X_{imp}, mm	β	Re_{Ximp}, 10^3	δ^*, mm	State of BL
1.42	0.694	286.4	10.92	288	3°, 4°	3146	0.53	Turb.
1.42	0.847	280.8	13.71	290	4°	3974	0.425	Turb.
1.42	0.984	284.2	15.65	290	4°	4539	0.458	Turb.
1.43	0.553	284.7	8.77	183	4°	1604	-	Tran.
1.43	0.688	284.5	10.91	183	3°, 4°	1997	0.369	Tran.
1.43	0.841	285.6	13.27	183.5	4°	2435	0.309	Tran.
1.43	0.976	286.5	15.32	183.5	4°	2812	0.239	Tran.
1.43	0.551	291	8.48	132	4°	1119	0.3	Lam.
1.43	0.694	290.4	10.70	133	3°, 4°	1423	0.27	Lam.
1.43	0.834	286.3	13.11	134	4°	1757	0.25	Lam.
1.43	0.978	285.1	15.46	134	4°	2072	0.22	Lam.

For quantitative comparisons of the test cases it was decided to obtain density and pressure distributions from PIV data by using of stationary Navier-Stokes equations. To simplify their solutions, it was assumed that at the stagnation enthalpy (but not its integral) is constant everywhere in the domain. This assumption is incorrect in the shear layer, but the error due to this assumption does not exceed 1-3%. For the left boundary condition the static pressure in the free stream was used. Pressure at the upper boundary was obtained using the law of mass conservation along the streamline.

$$\begin{cases} \dfrac{\partial \rho u}{\partial x}+\dfrac{\partial \rho v}{\partial y}=0 \\ \rho u\dfrac{\partial u}{\partial x}+\rho v\dfrac{\partial u}{\partial y}=-\dfrac{\partial P}{\partial x}+\mu\left(\dfrac{\partial^2 u}{\partial x^2}+\dfrac{\partial^2 u}{\partial y^2}\right)+\dfrac{\mu}{3}\dfrac{\partial}{\partial x}\left(\dfrac{\partial u}{\partial x}+\dfrac{\partial v}{\partial y}\right) \\ \rho u\dfrac{\partial v}{\partial x}+\rho v\dfrac{\partial v}{\partial y}=-\dfrac{\partial P}{\partial y}+\mu\left(\dfrac{\partial^2 v}{\partial x^2}+\dfrac{\partial^2 v}{\partial y^2}\right)+\dfrac{\mu}{3}\dfrac{\partial}{\partial y}\left(\dfrac{\partial u}{\partial x}+\dfrac{\partial v}{\partial y}\right) \\ c_p T+\dfrac{\left(u^2+v^2\right)}{2}=c_p T_0 \end{cases}$$

Figure 3 shows the static pressure distributions corresponding to the data presented in Figure 2. The correctness of the calculated pressure is proved by coincidence of pressure rise through the shock wave generated by the wedge with its theoretical value. Moreover on the pressure distributions one can find the characteristic features of SWBLI. For example, let's consider Figure 3b. The first growth of the pressure in the inviscid flow takes place at the shock wave generated by the wedge. In the shear layer the adverse pressure gradient extends upstream and increases the displacement thickness. This generates a reflected (separation) shock wave, which leads to further increase of pressure in the inviscid flow. Shock wave (generated by a wedge) is reflected from the boundary layer as a set of expansion waves, which leads to reduction of pressure. The increase of pressure near the end of zone of SWBLI occurs due to the shock wave caused by the turning of the streamlines parallel to the wall.

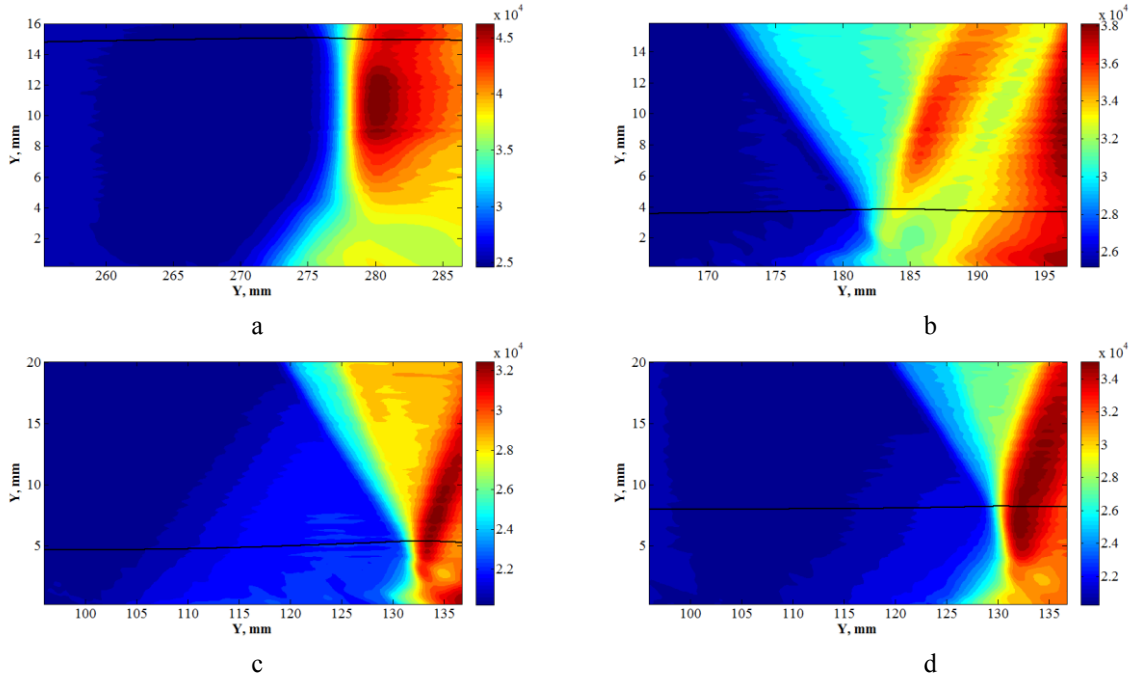

Figure 3 Pressure fields for different inflow boundary layers: a) turbulent, b) transitional, c) laminar, d) laminar with roughness

Analysis of the mean parameters of the SWBLI zone was carried out in paper [8]. It was shown that the best mean parameters of SWBLI are achieved when the inflow boundary layer have the transitional state. Turbulent case has no advantages in comparison with laminar, therefore from this point of view, using of roughness for the laminar flow is not necessary. Though the paper [8] considered only the data obtained in the zone of interaction, the increase of pulsations downstream for the case of inflow laminar boundary layer was niticed. Let's consider the distribution of unsteady parameters in the zone of interaction and wake.

Using the RMS values of pulsations of the longitudinal component of the velocity the following value can be calculated: $\int \rho < u >^2 dy$ (Figure 4). The integral calculated along the normal coordinate up to the undisturbed inviscid flow (black line in Figure 3). This value will be analyzed coupled with momentum thickness distribution along the zone of interaction (Figure 5).

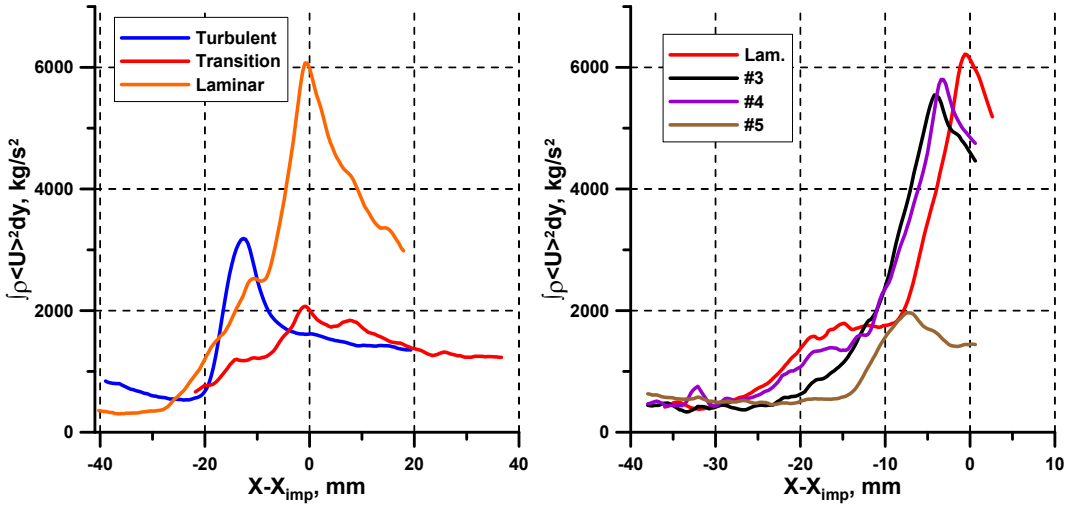

a b

Figure 4 The integrated RMS velocity fluctuation along the SWBLI a – natural conditions for $Re_1 = 13.2 \cdot 10^6$ m^{-1} and b – for different types of turbulators, $Re_1 = 10.7 \cdot 10^6$ m^{-1}

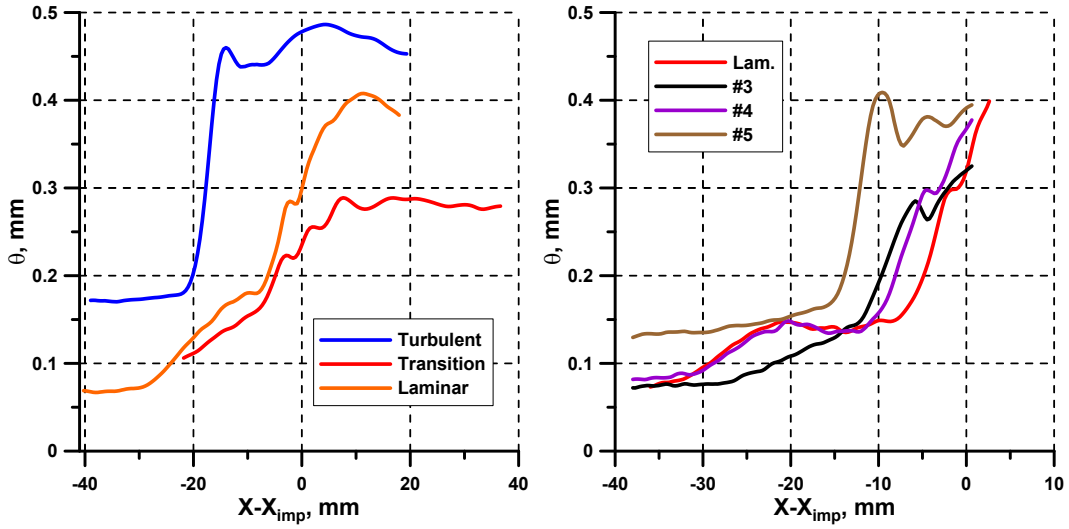

a b

Figure 5 The momentum thickness distribution along the SWBLI a – natural conditions for $Re_1 = 13.2 \cdot 10^6$ m^{-1} and b – different types of turbulators, $Re_1 = 10.7 \cdot 10^6$ m^{-1}

For the turbulent inflow boundary layer (Figure 4a) the peak of pulsations is found at the beginning of the zone of SWBLI near the reflected shock wave. Near this location there are largest increase of displacement thickness and loss of stagnation pressure. It is obvious that the growth of pulsations is a result of convective processes and energy transfer in the shear layer which leads to increase of drag.

Increasing the pulsations for the transitional case is much smaller and accompanied by weaker growth of momentum thickness. For the laminar case the most dramatic growth of pulsations (more than in turbulent case) is detected. This is accompanied by an increase of momentum thickness approximately up to the level of turbulent case. It can be assumed that further downstream the momentum thickness for the laminar case will be larger than in turbulent case due to greater value of the pulsation. Therefore despite the similar losses in the zone of SWBLI for laminar and turbulent case, probably the loss of total pressure for laminar case in the wake will be larger. It is necessary to perform additional measurements in the wake zone to clarify this question. It should be also noted that due to low

spatial resolution of the PIV method (for the selected scale), the momentum thickness for the laminar and transitional inflow boundary layer is overestimated.
In Figure 4b and Figure 5b one can see the effect of the turbulators. It is clearly seen that the difference between the turbulent (# 5) and the laminar case become smaller in comparison with Figure 4a and Figure 5a. The data obtained for the turbulators, which do not cause immediate laminar-turbulent transition upstream of the interaction zone, are more or less similar to the laminar case. The momentum thickness for the natural laminar case at the end of the measurement area is close to the turbulent regime but continues to grow. Therefore, the use of the turbulators can be useful to improve the flow parameters in the wake zone.

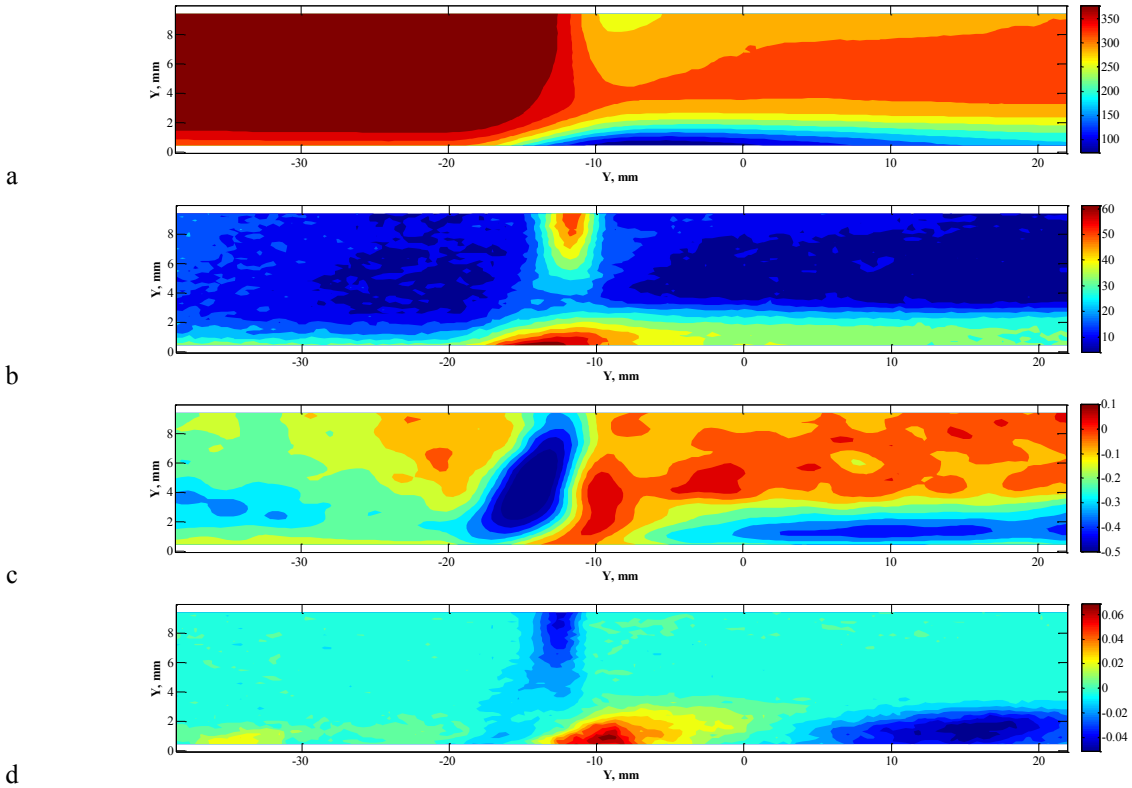

Figure 6 a) Mean velocity, b) RMS of longitudinal velocity, c) correlation coef. R_{UV}, d) example of POD modes for turbulent inflow boundary layers ($Re_1 = 13.2 \cdot 10^6$ m^{-1})

In Figure 6-Figure 8 show the distributions of mean velocity, RMS of longitudinal velocity, the correlation coefficient R_{UV} and the example of the POD analysis for the case of a turbulent, transitional and laminar inflow boundary layer. It is clearly seen that for the turbulent case (Figure 6b) the pulsation of the zone of interactions leads to oscillations of the Mach stem. It was found that in the logarithmic part of the incoming equilibrium turbulent boundary layer the coefficient $R_{UV} \approx$-0.2. In the zone of SWBLI the R_{UV} significantly deviates from this value. In this zone non-equilibrium turbulent boundary layer occurs, but further downstream the correlation coefficient begins to recover. At the end of the measurement domain the coefficient $R_{UV} \approx$-0.3. Example of POD modes (Figure 6d) shows the presence of interconnected characteristic oscillations across the domain. It can be seen that the oscillations of POD mode exist in the incoming boundary layer. Perhaps the large-scale structures in the zone of SWBLI and wake arise from the pulsations of the incoming boundary layer for turbulent case.

a

b

c

d

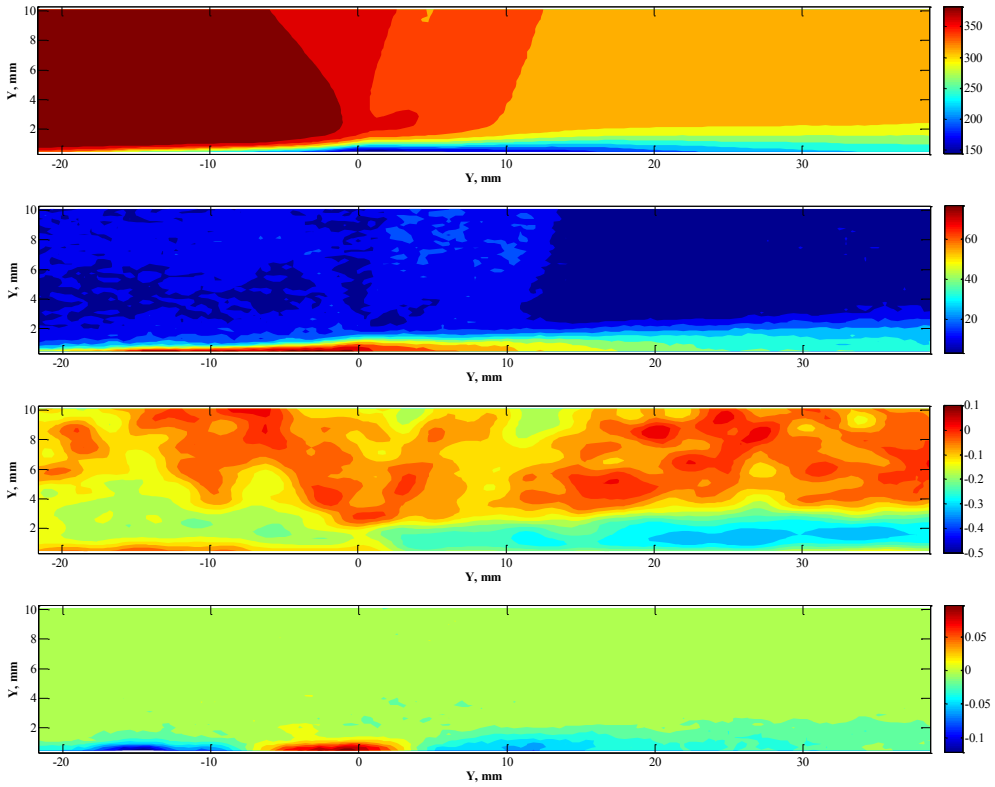

Figure 7 a) Mean velocity, b) RMS of longitudinal velocity, c) correlation coef. R_{UV}, d) example of POD modes for transition inflow boundary layers ($Re_1 = 13.2 \cdot 10^6$ m^{-1})

a

b

c

d

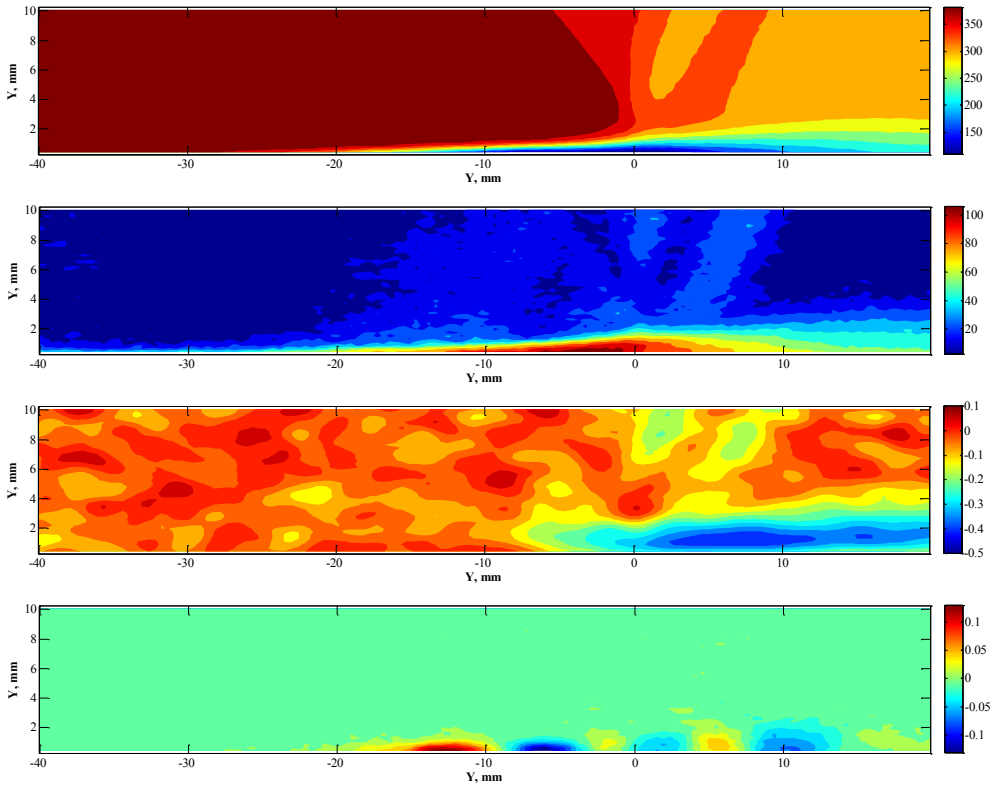

Figure 8 a) Mean velocity, b) RMS of longitudinal velocity, c) correlation coef. R_{UV}, d) example of POD modes for laminar inflow boundary layers ($Re_1 = 13.2 \cdot 10^6$ m^{-1})

In the case of laminar-turbulent transition (Figure 7) high level of pulsations was found only in the shear layer. In contrast to the turbulent case where the maximum of pulsations occurs near the reflected shock wave for the

transitional case the growth of pulsations is retained up to the point X_{imp} . Further downstream fullness of the velocity profile and absolute value of the coefficient R_{UV} begins to grow. It happens due to turbulization of the boundary layer. The coefficient R_{UV} near the end of the measured area is approximately equal to -0.2. This means that the turbulent boundary layer is rapidly restored to equilibrium state. For first twenty POD modes significant damping of unsteady processes was found near the end of the domain (see, for example, Figure 7d). The turbulent boundary layer arising in the zone of SWBLI for the transitional case quickly "forgets" about the interaction zone.

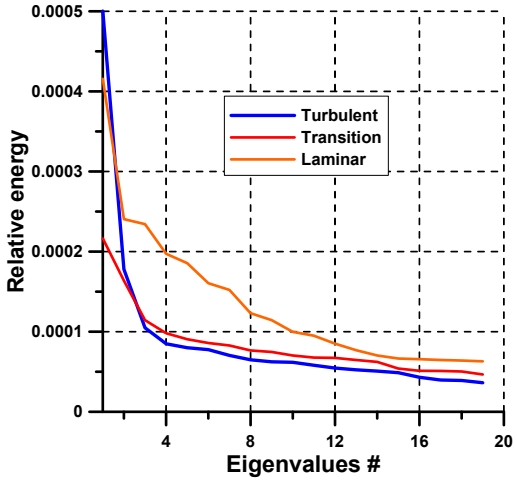

Figure 9 Relative energy associated with mode #m

For the laminar case the flow pattern is similar to the transition case, but there are several significant differences. First of all there is a significant growth of the pulsations and generation of thick turbulent boundary layer as a result. Absolut value of R_{UV} increases dramatically in the zone of interaction and begins to decrease downstream. A significant decrease of POD modes energy near the end of the measured zone was not found. It can be assumed that for the laminar case in the SWBLI zone strongly nonequilibrium turbulent boundary layer is generated with high level of RMS , which slowly recovers downstream. In the transitional case the process of the turbulization is more gradual.

In Figure 9 one can see the energy distribution for the first 20 modes obtained from POD analysis. The area of measurements for all cases was approximately the same, that allows to perform a quantitative comparison. The energy of structured oscillations of the flow for the laminar case significantly exceeds the values obtained for turbulent and transitional cases. Thus for laminar case the powerful coherent structures present in the interaction zone.

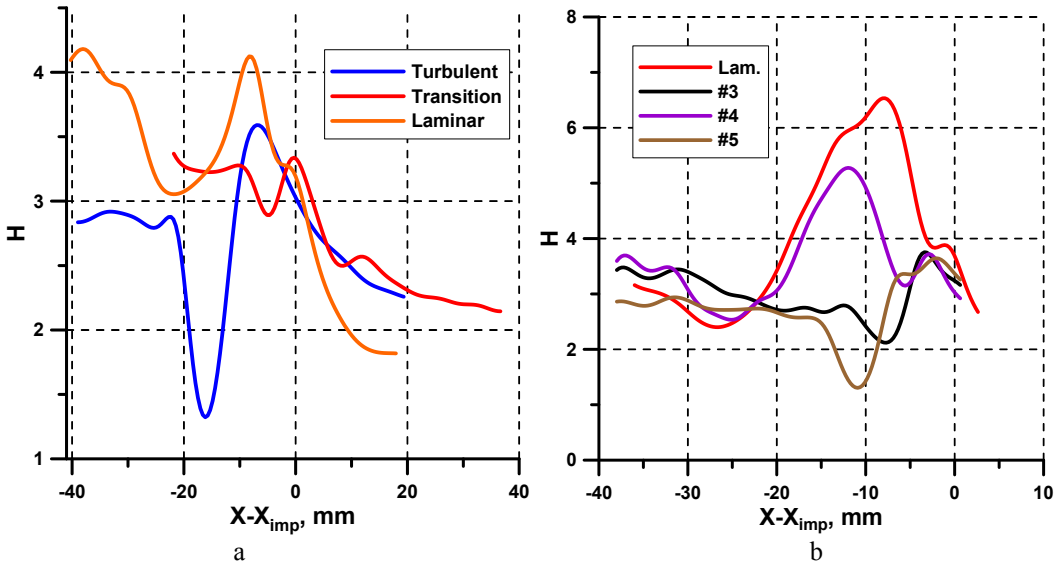

Figure 10 The shape factor along the SWBLI; a – natural conditions for $Re_1 = 13.2 \cdot 10^6$ m^{-1} and b – for different types of turbulators, $Re_1 = 10.7 \cdot 10^6$ m^{-1}

Distribution of the shape factor along the interaction zone is shown in Figure 10. For the transitional and turbulent case the values of the shape factors in the wake are similar and decrease downstream. The sharp decrease of H in the interaction zone occurs for the laminar case. It is assumed that it varies slightly further downstream. This can be explained by the different development of the boundary layer in the wake. To improve the knowledge about the characteristics of non-equilibrium turbulent boundary layer in wake for the laminar case the additional measurements were carried out. The result of measurements is shown in Figure 11. The solid line corresponds to the data obtained in the zone of interaction, the dotted line – to measurements in wake. It is clearly seen the match of the data obtained for the same flow conditions. Integral parameters (momentum thickness, shape factor) vary only slightly.
The evolution of the boundary layer in the wake is better seen from Figure 12. The velocity and velocity fluctuations distributions in the boundary layer at the end of the measuring area become closer to the equilibrium turbulent boundary layer. Since the momentum thickness in this wake varies weakly (Figure 11a) it can be assumed that the evolution of the boundary layer occurs only by redistribution of the energy accumulated in the zone of SWBLI. And the exchange of energy with the inviscid flow in the wake is weak. POD analysis shows weak damping of structures in the boundary layer in the wake.

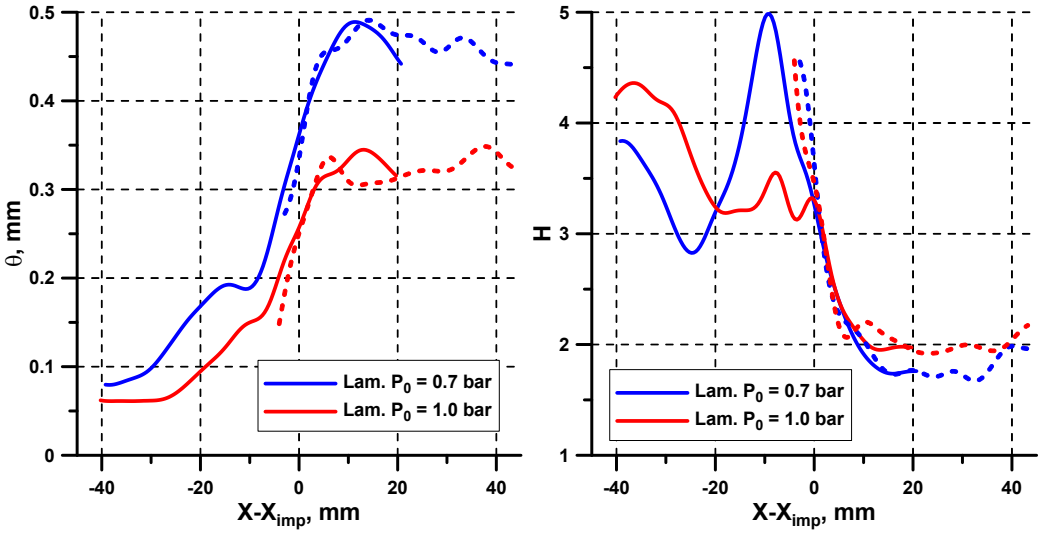

a b

Figure 11 a) The momentum thickness and b) shape factor distribution along the SWBLI

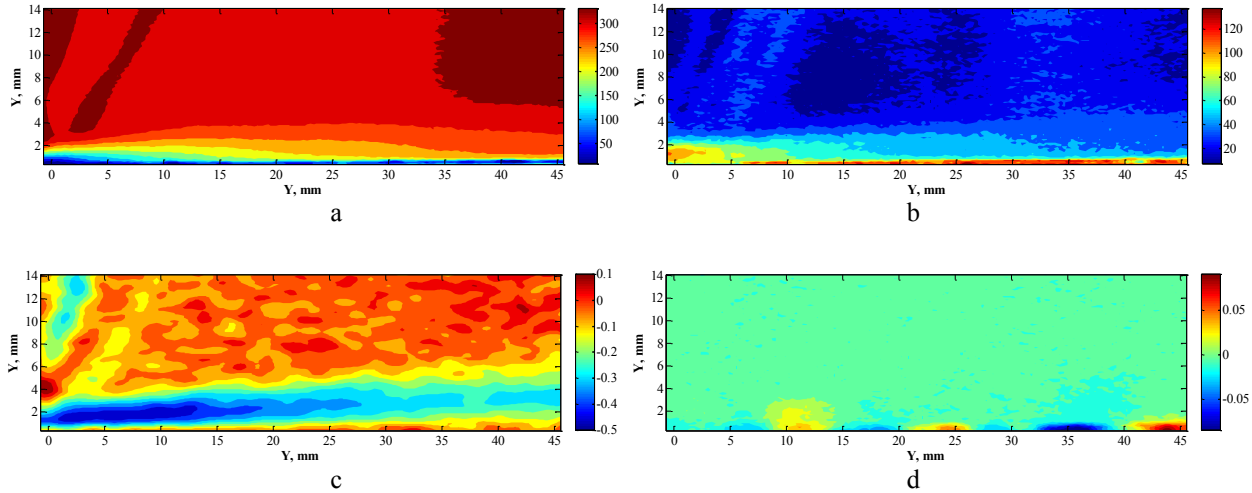

a b

c d

Figure 12 a) Mean velocity, b) RMS of longitudinal velocity, c) correlation coef. R_{UV} fields, d) example of POD modes in the wake of SWBLI for laminar inflow boundary layers ($Re_1 = 10.7 \cdot 10^6$ m^{-1})

Figure 13 shows the distribution of the wall pressure and momentum thickness for two angles of wedge 3° and 4°. The size of the interaction zone for the turbulent case decreases with decreasing of the wedge angle, but is

approximately unchanged for the laminar and transition cases. Most probably the size of the interaction zone for the laminar and transitional cases depends on the turbulization processes in the boundary layer.

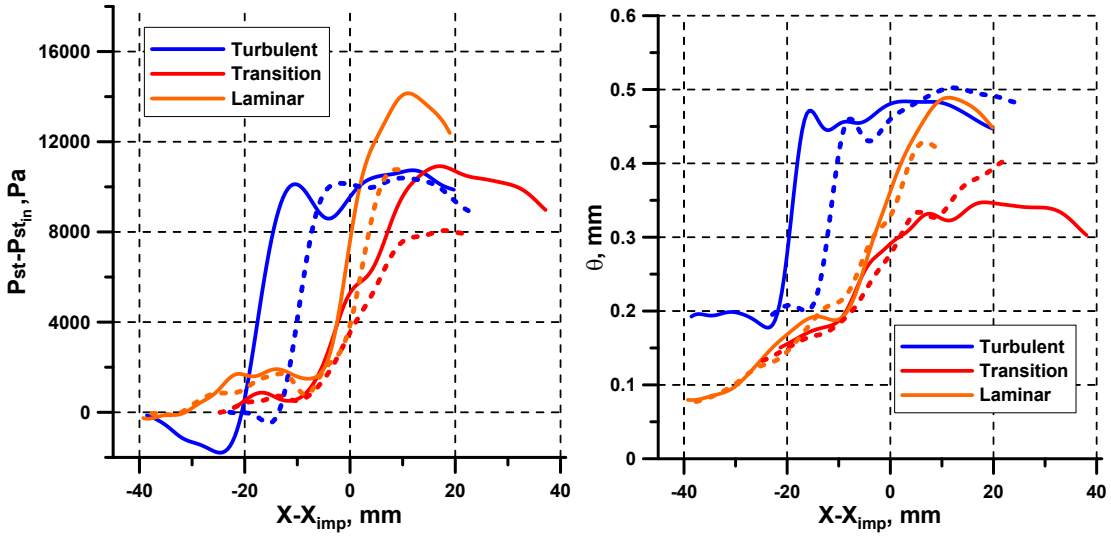

Figure 13 a) The wall pressure and b) momentum thickness distribution along the SWBLI (solid line $\beta = 4$, dash line $\beta = 3$)

3. Conclusions

It was found that the evolution of the turbulent boundary layer in the wake strongly depends on the state of the boundary layer upstream of SWBLI. It is shown that the effect of the angle of the incident shock wave on the flow depends on the state of the incoming boundary layer. It was found that for the laminar case the turbulent boundary layer generated in the zone of interaction quickly takes energy from the flow. It can be assumed that this energy is contained in the coherent structures. For the transitional case this effect was not found. As a result, the viscous losses for the transitional case are substantially less in comparison with the laminar and turbulent cases.

Acknowledgements

The work was supported by EU in framework of FP7 TFAST project and the Mega-grant of the Russian Federation Government to support scientific research under the supervision of leading scientist at Novosibirsk State University, No. 14.Z50.31.0019.

References

[1] E. Allison, I. Kroo, P. Sturdza, Y. Suzuki, H. Martins-Rivas. Aircraft Conceptual Design with Natural Laminar Flow. 27th International Congress Of The Aeronautical Sciences. 2010.
[2] J.E. Green. Laminar Flow Control - Back to the Future? AIAA Paper 2008-3738.
[3] B.H.K. Lee. Self-sustained shock oscillations on airfoils at transonic speeds. Progress in Aerospace Sciences. 2001. Vol. 37. P. 147-196.
[4] M. Swoboda and W. Nitschef. Shock Boundary-Layer Interaction on Transonic Airfoils for Laminar and Turbulent Flow. Journal of aircraft. 1996. Vol. 33. No. 1. P. 100-108.
[5] U. Cella, D. Quagliarella, R. Donelli and B. Imperatore. Design and Test of the UW-5006 Transonic Natural-Laminar-Flow Wing. Journal of aircraft. 2010. Vol. 47. No. P. 783-795.
[6] P.A. Polivanov, A.A. Sidorenko, A.A. Maslov. Correlation study in shock wave-turbulent boundary layer interaction // Shock Waves. 2011. Vol.21, No.3. P. 193-203.
[7] P.A. Polivanov, A.A. Sidorenko, A.A. Maslov. Receptivity of shock wave / turbulent boundary layer interaction to upstream disturbances // 45th Symposium of Applied Aerodynamics (France, Marseille, 22-24 March 2010): Proceedings. S.l., 2010. P. 1-10.

[8] P.A. Polivanov, A.A. Sidorenko, A.A. Maslov. Transition Effect on Shock Wave / Boundary Layer Interaction at M=1.47 // AIAA Paper 2015-1974.